IEEE Access
Multidisciplinary | Rapid Review | Open Access Journal

Received February 19, 2021, accepted April 15, 2021, date of publication April 26, 2021, date of current version May 5, 2021.

Digital Object Identifier 10.1109/ACCESS.2021.3075702

Evaluating the Mobility Impact on the Performance of Heterogeneous Wireless Networks Over $\eta - \mu$ Fading Channels

EKKAPHOT MEESA-ARD AND SUWAT PATTARAMALAI

Department of Electronic and Telecommunication Engineering, King Mongkut's University of Technology Thonburi, Bangkok 10140, Thailand

Corresponding author: Suwat Pattaramalai (suwat.pat@kmutt.ac.th)

This work was supported by the Department of Electronic and Telecommunication Engineering, Faculty of Engineering, King Mongkut's University of Technology Thonburi.

ABSTRACT The 5G and beyond networks will intrinsically accommodate a wide range of use-case scenarios and expand the limit of legacy mobile systems. The 5G network architecture can handle the seamless operation of various wireless channels in a heterogeneous environment. The η-μ fading model is well-suited for versatile channels as it adapts to different fading behaviors in a broad-range propagation for non-line-of-sight (NLOS) circumstances. This paper evaluates the performance of heterogeneous wireless networks using η-μ fading channel under mobility conditions. We incorporated the random waypoint (RWP) model with η-μ distribution to model the dynamic behavior of non-homogeneous fading. The derivation of expressions for the probability density function (PDF) and cumulative distribution function (CDF) of the received signal power for a mobile network in all three-dimensional topologies is extracted. Consequently, the outage probability (OP) and average bit error rate (ABER) are analyzed to quantify the performance of the mobile system. The effect of co-channel interference (CCI) is investigated based on a desired and interfering signal transmitted in mobile networks. The proposed novel-form can characterize the performance of a mobile user, and the derivation is useful for measuring the effect of noise and interference on the signal. Finally, the novel-form applicability analyzes the impact of mobility incorporated in different fading channels such as Nakagami-m, Nakagami-q (Hoyt), Rayleigh, and one-sided Gaussian distributions.

INDEX TERMS Co-channel interference, η-μ distribution, generalized fading model, heterogeneous network, random waypoint mobility.

I. INTRODUCTION

The performance evaluation of wireless networks is essential for improving the performance and development of next-generation networks such as 5G and 6G [1], [2]. Performance of the wireless network depends on several parameters that are statistically used to characterize the network's behavior. The received signal strength indications (RSSI) play a vital role in designing the channel assignment, handover, and power control and have been considered instrumental in enhancing the capacity and performance of wireless networks [3]. In existing studies, the statistical models assume the static characteristic of wireless networks [4]. However, with the advent of communication technologies such as IoT, 5G, and 6G, the network characteristic is becoming increasingly dynamic and complex [5]–[7]. The existing statistical model cannot accurately model the environment's dynamics due to the nodes' mobility characteristics. Thus, a research gap exists in developing the channel models that can perform well in mobile wireless networks.

The communication architectures such as 5G and 6G are expected to improve the network performance by achieving a high data rate in the dynamic and mobile environment. These architectures will have a dynamic network environment and stringent quality of service (QoS) requirements [8]. The applications of the latest communication architecture will have diverse and non-homogeneous characteristics of the received signal with line-of-sight (LOS) to NLOS conditions [9]. Statistical models are commonly used for characterizing the effects of fading in a wireless network. Several

The associate editor coordinating the review of this manuscript and approving it for publication was Yan Huo.

statistical models, including Nakagami-*m*, Rayleigh, Weibull, Nakagami-*q*, and Rician [10], [11] discuss short-term signal fluctuations.

The fading phenomenon can significantly improve the quality of signal reception in wireless networks. Conventional fading distributions are derived from the assumption that the scattering field in wireless communication has homogeneous characteristics [12]. However, this assumption is undoubtedly an approximation, as the networks that characterize heterogeneous environments have spatially correlated characteristics [13]. Different techniques have been successfully developed in stochastic geometry to model the heterogeneous characteristics of next-generation wireless networks. Stochastic geometry considers that the mobility characteristics of wireless nodes have a spatial point process [14]. This approach can capture the randomness in network topology and analyze the mathematical tools to achieve an accurate performance for the evaluation [15]. Moreover, conventional fading models lack the flexibility to model the signals propagating in complex and dynamic environments. Thus, mobile nodes in wireless networks need to consider both characteristics simultaneously to improve network performance.

η-μ Distribution is an essential generalized and flexible model capable of providing accurate approximations of the actual fading occurring in heterogeneous environments [16]. The model can predict the behavior of signals with multipath clusters, and its flexibility allows it to adapt to a wide range of field measurement data. Previous studies have characterized the η-μ fading model based on signal behavior in static conditions, providing a basic approach for these simplistic models and thereby allowing them to maintain tractability when analyzing OP, bit error rate, and channel capacity in such conditions [17]–[21]. Moreover, impact analyses of small-scale signal fluctuations in physical-layer signal propagation and end-to-end performance analyses of various complex network topologies were also described [22]–[26]. The behavior of the mentioned metrics of a signal propagating in the η-μ faded channel was also evaluated in the presence of co-channel interference [27]–[30].

For an effective characterization of channels, human and device mobility patterns need to be accurately predicted. Thus, it is important to investigate the relative locations in which mobile users are positioned [31], [32]. Mobility models can generate movement patterns from which parameters related to it are selected randomly. These characteristics are used in cellular and vehicular networks to predict user motion [33], [34]. Conventional models can be classified into several key types: random walk, random waypoint, Gauss–Markov, and fluid flow [35]. Among them, RWP mobility is well known for its ability to describe non-uniform spatial network distributions [36]–[39]. The model simplifies the three-dimensional mobility of users in communication service networks. Several analyses of fading models incorporating mobility have been adapted in studies conducted in homogeneous environments. The effect of mobility on the received power of a signal in Rayleigh faded and Nakagami-*m* faded channels was investigated in [40], [41]. To adapt to advanced interference and mobility management techniques, next-generation networks were required in [42]. In a recent work [43], the researchers derived a novel-form expression for modeling the fading characteristic using a Rician fading channel. In the work, the dynamic and mobility characteristics of wireless networks are not modeled in their derivation. On the other hand, their scenario for calculating the OP did not assume the interference and noise in deriving the novel-form expression. This reveals a research gap in existing techniques for modeling the fading characteristics of wireless environments.

Thus, for quantification purposes, the behavior of the networks for the signal to interference ratio (SIR) and signal to noise plus interference ratio (SINR) in a generalized fading environments needs to be evaluated for performance.

The focus of this work is evaluating the impact of mobility on generalized fading distributions to predict realistic approximations of fading concerning noise and interference. Additionally, due to the generalized and flexible characteristics of the distribution, homogeneous fading models, including Nakagami-*m* and Nakagami-*q* (Hoyt), can also be assessed for their performance with mobility.

The main contributions of this paper are as follows:

1) The η-μ generalized fading distribution that incorporates mobility characteristics for various small-scale fading effects, including non-homogeneous environments, NLOS conditions, and multipath clustering, is considered in this study.
2) A novel approach valid for all dimensional topologies was applied to evaluate the network performance for a generalized fading channel.
3) Novel-form expressions were derived and used to investigate the OP and ABER of the received signal power of a mobile user in the η-μ fading model.
4) The numerical results reveal that the derived novel-form expression exhibits the dynamics of fading characteristics in a wireless network when compared to benchmark schemes. Thus, network designers can carefully utilize the proposed derivation to reduce the effect of noise and interference on the signal.
5) Close approximations of Nakagami-*m*, Nakagami-*q* (Hoyt), Rayleigh, and one-sided Gaussian distribution models were obtained that analyzed the effect of mobility on different fading and homogeneous architectures. The results are also well-proved and evaluated numerically for the Nakagami-*m* architecture.

The paper is as follows: Section II provides a detailed description of the system and signal models and derives the PDF. Section III formulates the underlying problem. Section IV describes performance metrics, including OP and ABER, which are derived while extending the analysis to account for the presence of interference. Furthermore, in Section V, the numerical results of various fading characteristics are presented. These provide desirable insights into the performance of wireless system. Section VI concludes

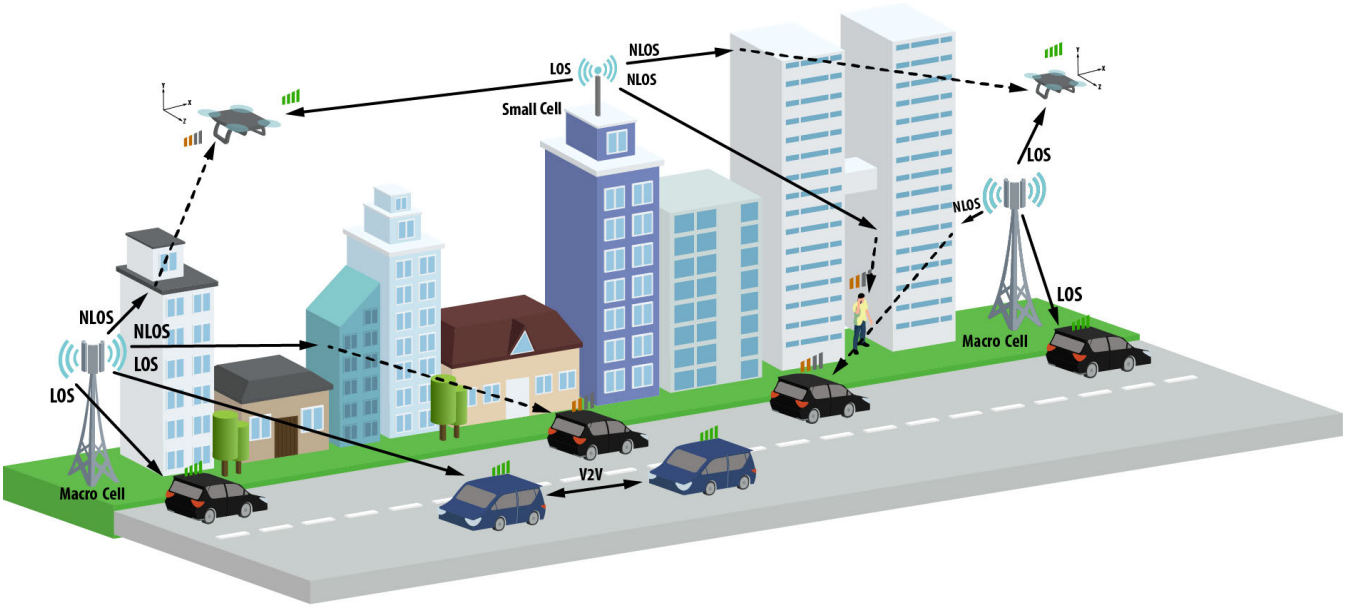

FIGURE 1. Schematic illustration of typical fading environments with mobility.

this work. Additionally, the appendix contains further information.

II. PROPOSED MODEL

Fig. 1 illustrates our proposed model which exhibits a dynamic environment comprising mobile vehicles and drones that can communicate in LOS and NLOS conditions. The nodes can move in 1-D, 2-D, and 3-D planes, and the handover phenomenon occurs while switching from one base station to another. The vehicles exhibit 1-D motion and the drones 3-D motion, each possessing different fading characteristics between LOS and NLOS environments. To model extreme wireless network conditions, the mobile nodes will also be subjected to path losses and co-channel interference. In the proposed model, two modes of communication are used: vehicle to vehicle (V2V), and vehicle to infrastructure (V2I). V2V handles normal communication while V2I is responsible for forwarding the data to infrastructure as illustrated in Fig. 1. To model the dynamics of fading in wireless networks, some vehicles receive data using the NLOS phenomenon while others use the LOS conditions. The drones communicate with the macro- and small-cell using the LOS and NLOS conditions. For the NLOS conditions, the signal reflects from the buildings while the LOS signals are received from the small and macro-cells. The proposed model flexibly models the dynamics of heterogeneous environments. The RWP mobility model is used for the movement of the nodes, while the η-μ distribution models the phenomenon of physical fading for its ability to approximate the characteristics of heterogeneous channel fading in dynamic environments. Besides these considerations, the important parameter that affects the quality of the received SNR is modeled for the fading characteristics. The drones and vehicles receive the signals under the interference and noise-with-interference scenarios.

III. PROBLEM FORMULATION

A. SIGNAL MODEL

We propose η-μ distribution to model the small-scale variation and dynamics in the fading signal. This distribution models the characteristics of well-known fading channels to exhibit next-generation communication networks such as IoT, 5G, and 6G. The PDF of instantaneous received power X of a signal transmitting in the η-μ fading distribution can be given by [44],

$$f_X(x) = \frac{2\sqrt{\pi}\mu^{\left(\mu+\frac{1}{2}\right)}h^{\mu}x^{\left(\mu-\frac{1}{2}\right)}}{\Gamma(\mu)H^{\left(\mu-\frac{1}{2}\right)}\Omega_r^{\left(\mu+\frac{1}{2}\right)}} \times exp\left[-\left(\frac{2\mu hx}{\Omega_r}\right)\right] I_{\mu-\frac{1}{2}}\left[\frac{2\mu Hx}{2}\right] \quad (1)$$

where μ represents the number of multipath clusters for the considered system while $I[.]$ is the modified Bessel function, and $\Gamma[.]$ stands for the gamma function. The H and h in equation (1) reflect the distribution parameters, with the η-μ distribution classified into two different physical representations parameters h, H and η are defined for both formats and can be seen in Appendix A.

To model the mobility characteristics in the proposed model, the average received power can be related to the separation of the transceiver using

$$\Omega_r = P_t r^{-\varphi} \quad (2)$$

where Ω_r and r represent the average power and separation of the transceiver. The $\varphi(2 \leq \varphi \leq 5)$ denotes the exponent of

TABLE 1. Polynomial coefficients [41].

Dimension	n	B_i	β_i
1	2	[6, −6]	[1, 2]
2	3	(1/73).[324, −420, 96]	[1, 3, 5]
3	3	(1/72).[735, −1190, 455]	[2, 4, 6]

path loss defined according to the characteristics of the proposed environment as shown in Fig. 1. P_t represents transmit power. The novel-form expressions derived in our paper also reflect the characteristics of the average received power.

It offers them the flexibility of application to fading environments with different path loss exponents.

In the proposed framework as shown in Fig. 1, a dynamic wireless network is considered to comprise mobile nodes where the destination nodes receive signals using LOS and NLOS conditions. To model the mobile nature of the IoT network, the propagation distance varies due to mobility. Conditional PDF can be obtained from equations (1) and (2) as follows:

$$f_X(x \mid r) = \left(\frac{2\sqrt{\pi}h^{\mu}}{\Gamma(\mu)}\right)\left(\frac{\mu}{P_t}\right)^{\left(\mu+\frac{1}{2}\right)}\left(\frac{x}{H}\right)^{\left(\mu-\frac{1}{2}\right)} \times r^{\varphi\left(\mu+\frac{1}{2}\right)} exp\left[-\left(\frac{2\mu hx}{P_t}r^{\varphi}\right)\right] \times I_{\mu-\frac{1}{2}}\left[\frac{2\mu Hx}{P_t}r^{\varphi}\right]. \quad (3)$$

Given a maximum range of D, the PDF in (3) is averaged to obtain the distribution of received power as follows:

$$f_X(x) = \int_0^D f_X(x \mid r) f_r(r) dr \quad (4)$$

where $f_r(r)$ is the PDF of separation distance r between the transmitter and receiver pair.

B. MOBILITY MODEL

A variety of mobility models associated with random movements are often represented using the statistical properties of randomness. Random direction (RD) and RWP are such models. Both are represented as polynomial functions of the separation of the transceiver in a steady state r. In this paper, the RWP mobility model was applied to approximate mobility. The spatial distribution of nodes in an RWP mobility model is non-uniform in general [34], and can be expressed by the polynomial in [40],

$$f_r(r) = \sum_{i=1}^{n} B_i \frac{r^{\beta_i}}{D^{\beta_i}+1}; \quad 0 \le r \le D. \quad (5)$$

Here, the distance of the transceiver is r. B_i and β_i are polynomial constants, and the upper limit of summation n depends on the dimension. By substituting the respective dimension-dependent polynomial coefficients 1-D, 2-D, and 3-D RWP, deployments can be obtained. The coefficients for different dimensional topologies are depicted in Table 1.

This analysis can be further extended and applied to any rotary symmetric spatial distribution that approximates polynomial functions.

In all three dimensions, it is assumed that the transmitter remains at the origin. In a 1-D scenario, it is in line with a transmitter placed at the origin, while for a 2-D and 3-D topology, it is a circular and spherical network. In the latter two dimensions, the transmitter is still considered to be located at the origin.

Then, by substituting (3) and (5) into (4), the following equation can be obtained:

$$f_X(x) = \int_0^D \left(\frac{2\sqrt{\pi}h^{\mu}}{\Gamma(\mu)}\right)\left(\frac{\mu}{P_t}\right)^{\left(\mu+\frac{1}{2}\right)}\left(\frac{x}{H}\right)^{\left(\mu-\frac{1}{2}\right)} \times r^{\varphi\left(\mu+\frac{1}{2}\right)} exp\left[-\left(\frac{2\mu hx}{P_t}r^{\varphi}\right)\right] \times I_{\mu-\frac{1}{2}}\left[\frac{2\mu Hx}{P_t}r^{\varphi}\right]\left(\sum_{i=1}^{n} B_i \frac{r^{\beta_i}}{D^{\beta_i+1}}\right) dr. \quad (6)$$

Now, the substitute to be solved is taken and the integral is simplified as

$$u = \left(\frac{r}{D}\right)^{\varphi}. \quad (7)$$

After modifying the integral variable applying the simplification process, the unconditional distribution can be represented in terms of received power as u using,

$$f_X(x) = \left(\frac{2\sqrt{\pi}h^{\mu}}{\varphi\Gamma(\mu)}\right)\left(\frac{\mu}{P_t}D^{\varphi}\right)^{\left(\mu+\frac{1}{2}\right)}\left(\frac{x}{H}\right)^{\left(\mu-\frac{1}{2}\right)} \times \sum_{i=1}^{n} B_i \int_0^1 u^{\left(\mu-\frac{1}{2}+\frac{(\beta_i+1)}{\varphi}\right)} \times exp\left[-\left(\frac{2\mu hxD^{\varphi}}{P_t}u\right)\right] I_{\mu-\frac{1}{2}}\left[\frac{2\mu HxD^{\varphi}}{P_t}u\right] du. \quad (8)$$

A modified Bessel function of the first kind can be expressed using a series summation as in [45] and can be represented as

$$I_v(z) = \sum_{m=0}^{\infty} \frac{1}{m!\Gamma(v+m+1)}\left(\frac{z}{2}\right)^{v+2m}. \quad (9)$$

Substituting the series in (9) into (8) and rearranging the result gives

$$f_X(x) = \left(\frac{2\sqrt{\pi}h^{\mu}}{\varphi\Gamma(\mu)}\right)\left(\frac{\mu}{P_t}D^{\varphi}\right)^{\left(\mu+\frac{1}{2}\right)}\left(\frac{1}{H}\right)^{\left(\mu-\frac{1}{2}\right)} \times \sum_{i=1}^{n} B_i \sum_{m=0}^{\infty} \frac{x^{2(\mu+m)-1}}{m!\Gamma\left(\mu+m+\frac{1}{2}\right)} \times \left(\frac{\mu hD^{\varphi}}{P_t}\right)^{\left(\mu+2m-\frac{1}{2}\right)} \int_0^1 u^{\left(2(\mu+m)+\left(\frac{\beta_i+1}{\varphi}\right)-1\right)} \times exp\left[-\left(\frac{2\mu hxD^{\varphi}}{P_t}u\right)\right] du. \quad (10)$$

The identity expressed in [45] is

$$\int_0^U x^{(v-1)} exp\left[-\mu x\right] dx = \mu^{-v}\gamma\left(v, \mu U\right). \tag{11}$$

where $\gamma(\cdot)$ is the incomplete gamma function of the first kind as in [45]. Thus, by taking (11) and further simplifying (10), the generalized novel-form expression for the PDF is

$$\begin{aligned} f_X(x) = &\left(\frac{1}{2}\right)^{(2\mu-1)} \left(\frac{\sqrt{\pi}}{\varphi\Gamma(\mu)}\right) \left(\frac{\Omega_0}{2\mu h}\right)^{\left(\frac{1}{\varphi}\right)} \left(\frac{1}{h}\right)^{\mu} \\ &\times \sum_{i=1}^{n} B_i \left(\frac{\Omega_0}{2\mu h}\right)^{\left(\frac{\beta_i}{\varphi}\right)} \\ &\times x^{-\left(\frac{\beta i+1}{\varphi}+1\right)} \sum_{m=0}^{\infty} \frac{1}{m!\Gamma\left(\mu+m+\frac{1}{2}\right)} \left(\frac{H}{2h}\right)^{2m} \\ &\times \gamma\left[2\left(\mu+m\right)+\left(\frac{\beta_i+1}{\varphi}\right), \frac{2\mu h x}{\Omega_0}\right] \end{aligned} \tag{12}$$

where $\Omega_0 = P_t D^{-\varphi}$ is the average received power observed at the boundary of the coverage area. Next, this study proceeded to evaluate the performance aspects in terms of OP and ABER on the basis of the derived PDF (12).

IV. PERFORMANCE ANALYSIS

A. OUTAGE PROBABILITY

The OP plays a vital role in designing and evaluating wireless networks. It represents the coverage area around the access node where the value of the received SNR is falls below a pre-defined threshold. This is shown as

$$\begin{aligned} P_{out} &= Pr\left[\theta < \theta_{thr}\right] \\ &= F_X\left(\theta_{thr}\right). \end{aligned} \tag{13}$$

where θ represents the value of the received SNR and θ_{thr} denotes the pre-defined threshold received SNR.

In a recent work [43], the authors considered a unity noise power for modeling the OP. In this work, considering a unity noise power, we formulated a closed-loop expression for the CDF as follows.

Transmit power is taken as a constant in mobile networks while, due to the mobility characteristics, the propagation constant is taken as a random variable. The received power can be calculated by averaging the range of distances over the PDF of random distance x, as the integration of the PDF over the range of distance yields the CDF with mobility

$$F_X(x) = \int_0^x f_X(z)\, dz. \tag{14}$$

The RWP mobility model is considered for evaluating the impact of mobility in dynamic wireless networks. In the RWP model, the receiving mobile nodes are placed randomly at the selected coordinate points depending on the network topology characteristics. It is assumed in all network topologies that the transmitter is located at the origin. The PDF of the distance x, assuming the RWP mobility model, can be viewed in [46].

The equation of the PDF as in equation (8) can be substituted into equation (14) to obtain the CDF of the received power as

$$\begin{aligned} F_X(x) = &\int_0^x \left(\frac{2\sqrt{\pi}h^{\mu}}{\varphi\Gamma(\mu)}\right) \left(\frac{\mu}{P_t}D^{\varphi}\right)^{\left(\mu+\frac{1}{2}\right)} \left(\frac{1}{H}\right)^{\left(\mu-\frac{1}{2}\right)} \\ &\times \sum_{i=1}^{n} B_i \sum_{m=0}^{\infty} \frac{z^{2(\mu+m)-1}}{m!\Gamma(\mu+m+\frac{1}{2})} \left(\frac{\mu h D^{\varphi}}{P_t}\right)^{\left(\mu+2m-\frac{1}{2}\right)} \\ &\times \int_0^1 u^{\left(2(\mu+m)+\left(\frac{\beta_i+1}{\varphi}\right)-1\right)} \\ &\times exp\left[-\left(\frac{2\mu h z D^{\varphi}}{P_t}u\right)\right] du dz. \end{aligned} \tag{15}$$

We should also note that although (12), refers to the more refined closed form expression of PDF of instantaneous power, (8) is more feasible to be used in our simplification in (15). Rearranging the value of x in equation (15) with the variable z results in

$$\begin{aligned} F_X(x) = &\left(\frac{2\sqrt{\pi}h^{\mu}}{\varphi\Gamma(\mu)}\right) \left(\frac{\mu}{P_t}D^{\varphi}\right)^{\left(\mu+\frac{1}{2}\right)} \left(\frac{1}{H}\right)^{\left(\mu-\frac{1}{2}\right)} \\ &\times \sum_{i=1}^{n} B_i \sum_{m=0}^{\infty} \frac{1}{m!\Gamma(\mu+m+\frac{1}{2})} \left(\frac{\mu H D^{\varphi}}{P_t}\right)^{\left(\mu+2m-\frac{1}{2}\right)} \\ &\times \int_0^1 u^{\left(2(\mu+m)+\left(\frac{\beta_i+1}{\varphi}\right)-1\right)} \\ &\times \int_0^x z^{2(\mu+m)-1} exp\left[-\left(\frac{2\mu h D^{\varphi}}{P_t}z\right)\right] dz du. \end{aligned} \tag{16}$$

After simplifying the equation (16) and using the integral in equation (11) including the value of z, the equation can be transformed into a gamma function as

$$\begin{aligned} F_X(x) = &\left(\frac{2\sqrt{\pi}h^{\mu}}{\varphi\Gamma(\mu)}\right) \left(\frac{\mu}{P_t}D^{\varphi}\right)^{\left(\mu+\frac{1}{2}\right)} \left(\frac{1}{H}\right)^{\left(\mu-\frac{1}{2}\right)} \\ &\times \sum_{i=1}^{n} B_i \sum_{m=0}^{\infty} \frac{1}{m!\Gamma(\mu+m+\frac{1}{2})} \\ &\times \left(\frac{\mu H D^{\varphi}}{P_t}\right)^{\left(\mu+2m-\frac{1}{2}\right)} \int_0^1 u^{\left(2(\mu+m)+\left(\frac{\beta_i+1}{\varphi}\right)-1\right)} \\ &\times \left[\frac{2\mu h D^{\varphi} u}{P_t}\right]^{-2(\mu+m)} \\ &\times \gamma\left[2\left(\mu+m\right), \frac{2\mu h D^{\varphi} x}{P_t}u\right] du. \end{aligned} \tag{17}$$

The relationship of average received power $\Omega_0 = P_t D^{-\varphi}$ can then be used to simplify and rearrange (17) further to

obtain

$$F_X(x) = \left(\frac{2\sqrt{\pi}h^{\mu}}{\varphi\Gamma(\mu)}\right)\left(\frac{\mu}{\Omega_0}\right)^{\left(\mu+\frac{1}{2}\right)}\left(\frac{1}{H}\right)^{\left(\mu-\frac{1}{2}\right)} \times \sum_{i=1}^{n} B_i \sum_{m=0}^{\infty} \frac{1}{m!\Gamma(\mu+m+\frac{1}{2})} \times \left(\frac{\mu H}{\Omega_0}\right)^{\left(\mu+2m-\frac{1}{2}\right)} \left[\frac{\Omega_0}{2\mu h}\right]^{2(\mu+m)} \times \int_0^1 u^{\left(\left(\frac{\beta_i+1}{\varphi}\right)-1\right)} \times \gamma\left[2(\mu+m), \frac{2\mu h x}{\Omega_0}u\right] du. \quad (18)$$

Using integration by parts, it can be shown for $v > 0$ that,

$$\int_0^1 x^{v-1}\gamma(m, ax)dx = v^{-1}[\gamma(m, a) - a^{-v}\gamma(v+m, a)]. \quad (19)$$

Then, using (19) and general simplifications, the novel-form expression for the CDF is obtained as

$$F_X(x) = \left(\frac{2^{(1-2\mu)}\sqrt{\pi}}{h^{\mu}\Gamma(\mu)}\right) \times \sum_{i=1}^{n} \frac{B_i}{(\beta_i+1)} \sum_{m=0}^{\infty} \frac{1}{m!\Gamma(\mu+m+\frac{1}{2})} \left(\frac{H}{2h}\right)^{2m} \times \left\{\gamma\left[2(\mu+m), \frac{2\mu h x}{\Omega_0}\right] - \left(\frac{2\mu h x}{\Omega_0}\right)^{-\left(\frac{\beta_i+1}{\varphi}\right)} \times \gamma\left[2(\mu+m) + \frac{\beta_i+1}{\varphi}, \frac{2\mu h x}{\Omega_0}\right]\right\}. \quad (20)$$

This equation (20) shows an important relationship for studying the OP in dynamic networks where $P_{out} = F_x(\lambda_{th})$ where λ_{th} is the pre-defined threshold.

B. AVERAGE BIT ERROR RATE

The ABER can be defined as the number of bits received in a unit time in data transmitting over a channel.

The data is being transmitted in noisy and distorted channels. The ABER for binary modulations in a fading channel expressed in [47] is

$$\bar{P_b} = \frac{a^b}{2\Gamma(b)} \int_0^{\infty} x^{b-1} e^{-ax} F_X(x)\, dx \quad (21)$$

where a and b are constants that depend on the modulation type as given in [48]. Table 2 which provides the modulation with constant values.

The expression of the CDF incorporating the mobility characteristics is substituted from (20) into (21) resulting in the ABER distribution, which can be expressed as

$$\bar{P_b} = \left(\frac{2^{(1-2\mu)}\sqrt{\pi}}{h^{\mu}\Gamma(\mu)}\right) \sum_{i=1}^{n} \frac{B_i}{(\beta_i+1)} \times \sum_{m=0}^{\infty} \frac{1}{m!\Gamma(\mu+m+\frac{1}{2})} \left(\frac{H}{2h}\right)^{2m}$$

TABLE 2. Different modulation schemes showing values of *a, b*.

Modulation Type	a	b
BPSK	1	$\frac{1}{2}$
M-PAM	$\frac{2(M-1)}{M}$	$\frac{M^2-1}{6}$
M-PSK	2	$\frac{1}{2\sin^2\left(\frac{\pi}{M}\right)}$
M-QAM	$\frac{4(\sqrt{M}-1)}{\sqrt{M}}$	$\frac{M-1}{3}$

$$\times \frac{a^b}{2\Gamma(b)} \left\{\int_0^{\infty} x^{b-1} e^{-ax} \gamma\left[2(\mu+m), \frac{2\mu h x}{\Omega_0}\right] dx \times \int_0^{\infty} x^{b-1} e^{-ax} \left(\frac{2\mu h x}{\Omega_0}\right)^{-\left(\frac{\beta_i+1}{\varphi}\right)} \times \gamma\left[\frac{\beta_i+1}{\varphi} + 2(\mu+m), \frac{2\mu h x}{\Omega_0}\right] dx\right\}. \quad (22)$$

Then, the ABER can be expressed in terms of two functions as

$$\bar{P_b} = \frac{2^{(1-2\mu)}\sqrt{\pi}}{h^{\mu}\Gamma(\mu_d)} \sum_{i=1}^{n} \frac{B_i}{\beta_i+1} \sum_{m=0}^{\infty} \frac{1}{m!\Gamma(\mu+m+\frac{1}{2})} \times \left(\frac{H}{2h}\right)^{2m} \frac{a^b}{2\Gamma(b)} \{R_1 - R_{2i}\}. \quad (23)$$

Let R_1 in (23) be

$$R_1 = \int_0^{\infty} x^{b-1} e^{-ax} \gamma\left[2(\mu+m), \frac{2\mu h x}{\Omega_0}\right] dx. \quad (24)$$

Consider the identity expressed in [45] equation (6.455.2)

$$\int_0^{\infty} x^{\mu-1} e^{-\beta x} \gamma(v, ax)\, dx = \frac{a^v \Gamma(\mu+v)}{v(a+\beta)^{\mu+v}} \times {}_2F_1\left(1, \mu+v; v+1; \frac{a}{a+\beta}\right) \quad (25)$$

where ${}_2F_1(.,.;.;.)$ is the Gauss hypergeometric function, expressed in an integral form in [45] equation (9.111). Using (25), the integral of R_1 in (24) can be expressed in terms of the Gamma function and Gauss hypergeometric function. Then, the reduced form is given by

$$R_1 = \frac{\Gamma(b+2(\mu+m))}{2(\mu+m)} \left[\frac{2\mu h}{2\mu h + \Omega_0 a}\right]^{2(\mu+m)} \left[\frac{\Omega_0}{2\mu h + \Omega_0 a}\right]^{b} \times {}_2F_1\left(1, b+2(\mu+m); 2(\mu+m)+1; \frac{2\mu h}{2\mu h + \Omega_0 a}\right). \quad (26)$$

R_{2i} can be defined as

$$R_{2i} = \int_0^{\infty} x^{b-1} e^{-ax} \left(\frac{2\mu h x}{\Omega_0}\right)^{-\left(\frac{\beta_i+1}{\varphi}\right)} \times \gamma\left[\frac{\beta_i+1}{\varphi} + 2(\mu+m), \frac{2\mu h x}{\Omega_0}\right] dx. \quad (27)$$

Upon following the same process as for R_1, the simplified version for R_{2i} can be expressed in the following form:

$$R_{2i} = \frac{\Gamma\left(b+2\left(\mu+m\right)\right)}{\left(\frac{\beta_i+1}{\varphi}+2\left(\mu+m\right)\right)}\left[\frac{2\mu h}{2\mu h+\Omega_0 a}\right]^{2(\mu+m)} \times \left[\frac{\Omega_0}{2\mu h+\Omega_0 a}\right]^{b} \times {}_2F_1\left(1, b+2\left(\mu+m\right); \left(\frac{\beta_i+1}{\varphi}\right) +2\left(\mu+m\right)+1; \frac{2\mu h}{2\mu h+\Omega_0 a}\right). \quad (28)$$

R_1 and R_{2i} from equation (27) and (28) into (23) results in the ABER in novel form as in (29), as shown at the bottom of the next page.

C. EFFECT OF INTERFERENCE

The evaluation of the impact of co-channel interference (CCI), which is considered an effective criterion for evaluating the performance of the mobile user in the network, is reported in this section. The phenomenon is observed as a function of average and instantaneous SIR where the random effects of noise can be ignored. Thus, it is necessary to model the characteristics of SIR to analyze the effective performance of the observed system. The proposed model considers the dynamic characteristics of the environment by considering the effect of multipath fading by the η-μ fading model. The propagation characteristics of the desired signal and the occurrence of CCI are modeled as random processes. Due to the consideration of the interfering signal, from here onward, we use two distinct variable sets to represent both interference and desired signals instead of one. As detailed below, we use two variables μ_c and μ_d to represent the number of multipath clusters associated with the interfering signal and desired signal instead of μ.

The derived desired signal follows the CDF in (20), where $\Omega^0 = P_t D^{-\varphi}$ is the average received power of the desired signal and μ_d associates with the number of multipath clusters through which the desired signal is propagating [44]. In particular, $\mu_d > 0$ is the ratio between the total power of the scattered waves and that of the dominant components in the desired signal.

In CCI analysis, it is assumed that the interferers are located at identical distances from the mobile station. These are η-μ faded and are kept stationary throughout the analysis. Using the PDF of resultant interference signal given in [44], equation (5.22), Laplace transforms, and expression of the Bessel function with the series summation in (9) (similar to Section III-A), the PDF of the resultant interfering signal power can be given as

$$f_I\left(x\right) = \frac{2\sqrt{\pi}h^{\mu_c L}}{\Gamma\left(\mu_c L\right)}\left(\frac{\mu_c}{\Omega_I}\right)^{2\mu_c L}\sum_{m=0}^{\infty}\left(\frac{\mu_c H}{\Omega_I}\right)^{2m} \times \frac{1}{m!\Gamma(\mu_c L+m+\frac{1}{2})} \times x^{(2\mu_c L+2m-1)}exp\left[-\left(\frac{2\mu_c h}{\Omega_I}x\right)\right] \quad (30)$$

with $\Omega_I = P_I d^{-\varphi}$, representing the CCI signal average power and d is the separation between interferer and receiver. L is the number of interferers. The μ_c shows the number of multipath clusters through which the interfering signal is propagating [44]. Particularly, the $\mu_c > 0$ represents the ratio between the total power of the dominating components to the total power of the waves scattered in the interfering signal parameter representing the multipath clusters through which the interferer signal is propagating [49]. Then, the OP can be related as

$$P_{out}^{SIR} = Pr\left\{\frac{X}{I} \le \theta\right\} = E_I\left[F_X\left(\theta I\right)\right] \quad (31)$$

where X is the signal power and I is the aggregate interferer power; θ stands for the predefined threshold, and $E_I\left[\cdot\right]$ is the statistical expectation with respect to the random variable I. Using the derived CDF in (20) and combining it with the results of (31), we get

$$P_{out}^{SIR} = \frac{2^{(1-2\mu_d)}\sqrt{\pi}}{h^{\mu_d}\Gamma(\mu_d)}\sum_{i=1}^{n}\frac{B_i}{(\beta_i+1)}\sum_{m=0}^{\infty}\left(\frac{H}{2h}\right)^{2m} \times \frac{1}{m!\Gamma(\mu_d+m+\frac{1}{2})} \times E_I\left\{\gamma\left[2\left(\mu_d+m\right), \left(\frac{2\mu_d h\theta I}{\Omega_0}\right)\right] - \left(\frac{2\mu_d h\theta I}{\Omega_0}\right)^{-\left(\frac{\beta_i+1}{\varphi}\right)} \times \gamma\left[2\left(\mu_d+m\right)+\frac{\beta_i+1}{\varphi}, \left(\frac{2\mu_d h\theta I}{\Omega_0}\right)\right]\right\} \quad (32)$$

The expression in (32) can be expressed as the difference between two functions.

$$P_{out}^{SIR} = \frac{2^{(1-2\mu_d)}\sqrt{\pi}}{h^{\mu_d}\Gamma(\mu_d)}\sum_{i=1}^{n}\frac{B_i}{\beta_i+1}\sum_{m=0}^{\infty}\frac{1}{m!\Gamma(\mu_d+m+\frac{1}{2})} \times \left(\frac{H}{2h}\right)^{2m}\left(C_1 - C_{2i}\right). \quad (33)$$

The statistical expectation can be related using the average of an infinite series. Using this relationship, C_1 can be expressed as

$$C_1 = \frac{2\sqrt{\pi}}{\Gamma(\mu_c L)}\left(\frac{\mu_c}{\Omega_I}\right)^{2\mu_c L}h^{\mu_c L} \times \sum_{m=0}^{\infty}\frac{1}{m!\Gamma(\mu_c L+m+\frac{1}{2})}\left(\frac{\mu_c H}{\Omega_I}\right)^{2m} \times \int_0^{\infty}x^{(2\mu_c L+2m-1)}exp\left[-\left(\frac{2\mu_c h}{\Omega_I}x\right)\right] \times \gamma\left[2\left(\mu_d+m\right), \frac{2\mu_d h\theta x}{\Omega_0}\right]dx. \quad (34)$$

It should be noted that (34) inherits both the desired signal and the interfering signal due to the characteristic relationship in (31). Out of this, x is a random variable showing the desired

TABLE 3. Minimum number of terms of (37) needed to obtain accuracy better than $\pm 10^{-5}$ in the infinite series.

	Norm. Power = 5 dBm	Norm. Power = 10 dBm
$\mu_c = \mu_d = 1.5$		
$\eta = 0.5$	4	4
$\eta = 1.5$	7	6
$\mu_d = \mu_c = 2.5$		
$\eta = 0.5$	4	4
$\eta = 1.5$	7	7

signal and I is a random variable representing the resultant interfering signal. For example, the previously defined variables, including μ_c and μ_d, Ω_I and Ω_0 characterizing the resultant interfering signal and desired signal, co-exist interchangeably in the equations here.

$$C_{2i} = \left(\frac{2\mu_d h\theta}{\Omega_0}\right)^{-\left(\frac{\beta_i+1}{\varphi}\right)} \frac{2\sqrt{\pi}}{\Gamma(\mu_c L)} \times \sum_{m=0}^{\infty} (H)^{2m} \frac{\Gamma\left(2\left(\mu_c L + \mu_d + 2m\right)\right)}{m!\Gamma(\mu_c L + m + \frac{1}{2})} \times \frac{\left(\frac{1}{h}\right)^{(\mu_c L+2m)}}{\left(2\left(\mu_d + m\right) + \frac{\beta_i+1}{\varphi}\right)} \times \left(\frac{2\mu_d}{2\mu_d + \frac{2\mu_c\Lambda}{\theta}}\right)^{2(\mu_d+m)} \left(\frac{2\mu_c}{\frac{2\mu_d\theta}{\Lambda} + 2\mu_c}\right)^{2(\mu_c L+m)} \times {}_2F_1\Bigg(1, 2\left(\mu_c L + \mu_d + 2m\right); \times 2\left(\mu_d + m\right) + \left(\frac{\beta_i+1}{\varphi}\right) + 1; \frac{2\mu_d}{2\mu_d + \frac{2\mu_c\Lambda}{\theta}}\Bigg). \quad (35)$$

Using the identity in [45] equation (6.455.2), the integral in (34) can be solved as follows (see Appendix B for details): where $\Lambda = \frac{\Omega_0}{\Omega_I}$ is the average SIR of an interferer. equations (35) and (36), as shown at the bottom of the next page, can be substituted into equation (33) to obtain the equation (37), as shown at the bottom of the next page.

Equation (37) shows the OP of an interference-limited system in terms of a converging series. The results of a convergence analysis of the infinite series with an accuracy defined by the given significant figures are in Table 3.

D. EFFECT OF INTERFERENCE AND NOISE

Consider the PDF of the interference power expressed in (30) and the CDF expressed in (20).

The OP with the SINR when noise is taken to be a unit and can be expressed by

$$\begin{aligned} P_{out}^{SINR} &= E_I\left[F_X\left(\theta\left(I+1\right)\right)\right] \\ &= \frac{2^{(1-2\mu_d)}}{h^{\mu_d}\Gamma(\mu_d)}\sqrt{\pi}\sum_{i=1}^{n}\frac{B_i}{(\beta_i+1)} \\ &\quad\times\sum_{m=0}^{\infty}\frac{1}{m!\Gamma(\mu_d+m+\frac{1}{2})}\left(\frac{H}{2h}\right)^{2m} \\ &\quad\times E_I\Bigg[\gamma\left[2\left(\mu_d+m\right), \frac{2\mu_d h\theta}{\Omega_0}\left(I+1\right)\right] \\ &\quad- \left(\frac{2\mu_d h\theta}{\Omega_0}\left(I+1\right)\right)^{\frac{-(\beta_i+1)}{\varphi}} \\ &\quad\times\gamma\left[2\left(\mu_d+m\right)+\frac{(\beta_i+1)}{\varphi}, \frac{2\mu_d h\theta}{\Omega_0}\left(I+1\right)\right]\Bigg]. \end{aligned} \quad (38)$$

This can be separated into two functions for ease of understanding.

$$P_{out}^{SINR} = \frac{2^{(1-2\mu_d)}}{h^{\mu_d}\Gamma(\mu_d)}\sqrt{\pi}\sum_{i=1}^{n}\frac{B_i}{(\beta_i+1)}\sum_{m=0}^{\infty}\left(\frac{H}{2h}\right)^{2m} \times\frac{1}{m!\Gamma(\mu_d+m+\frac{1}{2})}\left(K_1-K_{2i}\right) \quad (39)$$

K_1 is simplified further and can be expressed as

$$\begin{aligned} K_1 &= \frac{2\sqrt{\pi}}{\Gamma(\mu_c L)}\left(\frac{\mu_c}{\Omega_I}\right)^{2\mu_c L} h^{\mu_c L} \\ &\quad\times\sum_{m=0}^{\infty}\frac{1}{m!\Gamma(\mu_c L+m+\frac{1}{2})}\left[\frac{\mu_c H}{\Omega_I}\right]^{2m} \\ &\quad\times\int_0^{\infty} x^{(2\mu_c L+2m-1)} exp\left(\frac{-2\mu_c h x}{\Omega_I}\right) \\ &\quad\times\gamma\left[2\left(\mu_d+m\right), \frac{2\mu_d h\theta}{\Omega_0}\left(x+1\right)\right]dx. \end{aligned} \quad (40)$$

The incomplete gamma function can be expressed in the integral form using the binomial expansion followed by

$$\begin{aligned} \bar{P_b} &= \frac{2^{(1-2\mu)}\sqrt{\pi}}{h^{\mu}\Gamma(\mu)}\sum_{i=1}^{n}\frac{B_i}{\beta_i+1}\sum_{m=0}^{\infty}\frac{1}{m!\Gamma(\mu+m+\frac{1}{2})}\left(\frac{H}{2h}\right)^{2m}\left[\frac{2\mu h}{2\mu h+\Omega_0 a}\right]^{2(\mu+m)} \\ &\quad\times\left[\frac{\Omega_0}{2\mu h+\Omega_0 a}\right]^{b}\Gamma\left(b+2\left(\mu+m\right)\right)\frac{a^b}{2\Gamma(b)}\Bigg\{\frac{1}{2\left(\mu+m\right)} \\ &\quad\times{}_2F_1\left(1, b+2(\mu+m); 2\left(\mu+m\right)+1; \frac{2\mu h}{2\mu h+\Omega_0 a}\right)-\frac{1}{\left(\frac{\beta_i+1}{\varphi}+2\left(\mu+m\right)\right)} \\ &\quad\times{}_2F_1\left(1, b+2\left(\mu+m\right); \left(\frac{\beta_i+1}{\varphi}\right)+2\left(\mu+m\right)+1; \frac{2\mu h}{2\mu h+\Omega_0 a}\right)\Bigg\} \end{aligned} \quad (29)$$

simplifications. According to Appendix B, it can be arranged into the form below.

$$K_1 = \frac{2\sqrt{\pi}}{\Gamma(\mu_c L)} h^{\mu_c L} \times \sum_{m=0}^{\infty} \frac{1}{m!\Gamma(\mu_c L + m + \frac{1}{2})} H^{2m} \sum_{j=0}^{2(\mu_d+m)} \binom{2(\mu_d+m)}{j} \times \left[\frac{2\mu_d h\theta}{\Omega_0}\right]^{2(\mu_d+m)} \left(\frac{\Omega_I}{\mu_c}\right)^j (2h)^{-2(\mu_c L+m)-j} \times \Gamma(2\mu_c L + 2m + j) \times \int_0^1 y^{2(\mu_d+m)-1} exp\left(-\left(\frac{2\mu_d h\theta}{\Omega_0}\right) y\right) \times \left[1-\left(\frac{-\mu_d \theta y}{\mu_c \Lambda}\right)\right]^{-2(\mu_c L+m)-j} (1-y)^{(1-1)}\, dy. \quad (41)$$

Here, m is the iteration variable of the summation series, which can take only integer values, and $(\mu_d+m) > 0$. To solve the integral in (41), consider the relationship expressed in [45] equation (3.385.1), which is of the same format.

$$\int_0^1 x^{(v-1)} (1-x)^{(\lambda-1)} (1-\beta x)^{-g} e^{-\mu x} dx = B(v,\lambda)\, \Phi_1[v, g, \lambda+v, \beta, -\mu] \quad (42)$$

Here, $B(\cdot)$ [45] equation (8.380.1) is the Beta function, and $\Phi_1(\cdot)$ is the confluent bivariate hypergeometric function defined in [45] equation (9.261.1).

Using the expression in (42) and the definition of a beta function, K_1 in (41) can be reduced to the simplified version expressed in (43) and refer to Appendix C for details.

$$K_1 = 2\sqrt{\pi} \sum_{m=0}^{\infty} \frac{1}{m!\Gamma(\mu_c L + m + \frac{1}{2})} H^{2m} \times \sum_{j=0}^{2(\mu_d+m)} \binom{2(\mu_d+m)}{j} \frac{\Gamma(2(\mu_c L+m)+j)}{\Gamma(\mu_c L)} \times \left[\frac{2\mu_d h\theta}{\Omega_0}\right]^{2(\mu_d+m)} \left(\frac{\Omega_I}{\mu_c}\right)^j \times \left(h^{-(\mu_c L+2m+j)}\right) 2^{-2(\mu_c L+m)} \frac{1}{(2\mu_d+m)} \times \Phi_1\left(2(\mu_d+m), 2(\mu_c L+m) + j, 2(\mu_d+m)+1, \left(\frac{-\mu_d\theta}{\mu_c\Lambda}\right), \frac{-2\mu_d h\theta}{\Omega_0}\right). \quad (43)$$

Following a similar process to that used for K_1, the integral of K_{2i} can be solved in terms of a confluent bivariate function, incomplete gamma function, gamma function, and binomial expansion to result in (44).

$$K_{2i} = \frac{2\sqrt{\pi}}{\Gamma(\mu_c L)} \sum_{m=0}^{\infty} \frac{1}{m!\Gamma(\mu_c L + m + \frac{1}{2})} \times \sum_{j=0}^{2(\mu_d+m)} \binom{2(\mu_d+m)}{j} h^{-\mu_c L-2m-j}$$

$$C_1 = \frac{2\sqrt{\pi}}{\Gamma(\mu_c L)} \sum_{m=0}^{\infty} \frac{H^{2m}\Gamma(2(\mu_c L+\mu_d+2m))}{2^{(2\mu_c L+2m+1)} m!\Gamma(\mu_c L+m+\frac{1}{2})(\mu_d+m) h^{\mu_c L+2m}} \times \left(\frac{2\mu_d}{2\mu_d+\frac{2\mu_c\Lambda}{\theta}}\right)^{2(\mu_d+m)} \left(\frac{2\mu_c}{\frac{2\mu_d\theta}{\Lambda}+2\mu_c}\right)^{2(\mu_c L+2m)} {}_2F_1\left(1, 2(\mu_c L+\mu_d+2m); 2(\mu_d+m)+1; \left(\frac{2\mu_d}{2\mu_d+\frac{2\mu_c\Lambda}{\theta}}\right)\right) \quad (36)$$

$$P_{out}^{SIR} = \frac{2^{(1-2\mu_d)}}{h^{\mu_d}\Gamma(\mu_d)} \sum_{i=1}^{n} \frac{B_i}{(\beta_i+1)} \sum_{m=0}^{\infty} \frac{1}{m!\Gamma(\mu_d+m+\frac{1}{2})} \left(\frac{H}{2h}\right)^{2m} \frac{2\sqrt{\pi}}{\Gamma(\mu_c L)} \times \sum_{m=0}^{\infty} \frac{(H)^{2m}\Gamma(2(\mu_c L+\mu_d+2m))}{m!\Gamma(\mu_c L+m+\frac{1}{2}) h^{\mu_c L+2m} 2^{(2\mu_c L+2m)}} \left(\frac{2\mu_d}{2\mu_d+\frac{2\mu_c\Lambda}{\theta}}\right)^{2(\mu_d+m)} \times \left(\frac{2\mu_c}{\frac{2\mu_d\theta}{\Lambda}+2\mu_c}\right)^{2(\mu_c L+m)} \left\{\frac{1}{2(\mu_d+m)} \times {}_2F_1\left(1, 2(\mu_c L+\mu_d+2m); 2(\mu_d+m)+1; \left(\frac{2\mu_d}{2\mu_d+\frac{2\mu_c\Lambda}{\theta}}\right)\right)\right. - \left(\frac{2\mu_d h\theta}{\Omega_0}\right)^{-\left(\frac{\beta_i+1}{\varphi}\right)} \frac{1}{\left(2(\mu_d+m)+\frac{\beta_i+1}{\varphi}\right)} \times {}_2F_1\left(1, 2(\mu_c L+\mu_d+2m); 2(\mu_d+m)+\left(\frac{\beta_i+1}{\varphi}\right)+1; \frac{2\mu_d}{2\mu_d+\frac{2\mu_c\Lambda}{\theta}}\right)\Bigg\} \quad (37)$$

TABLE 4. Minimum number of terms in (45) needed to obtain accuracy better than $\pm 10^{-5}$ in double infinite series.

	Norm. Power = 5 dBm	Norm. Power = 10 dBm
$\mu_c = \mu_d = 1.5$		
$\eta = 0.5$	4	4
$\eta = 1.5$	5	4
$\mu_d = \mu_c = 2.5$		
$\eta = 0.5$	4	4
$\eta = 1.5$	5	5

$$\times H^{(2m)}\Gamma\left(2\mu_c L+2m+j\right)2^{-2(\mu_c L+m)} \times\left(\frac{2\mu_d h\theta}{\Omega_0}\right)^{2(\mu_d+m)} \times\left(\frac{\Omega_I}{2\mu_c}\right)^{j}\frac{1}{\left(2\left(\mu_d+m\right)+\frac{\beta_i+1}{\varphi}\right)}\Phi_1 \times\left(2\left(\mu_d+m\right)+\frac{\beta_i+1}{\varphi},\right. 2\left(\mu_c L+m\right)+j, 2\left(\mu_d+m\right)+\frac{\beta_i+1}{\varphi}+1, \left.\left(\frac{-\mu_d\theta y}{\mu_c\Lambda}\right),\frac{-2\mu_d h\theta}{\Omega_0}\right). \quad (44)$$

Then, equations (43) and (44) can be substituted into (39) to get the OP in the presence of interference and noise. This can be expressed as a double infinite series that converges fast as shown in (45), as shown at the bottom of the page.

The number of terms that need to be summed for the series to converge for a result with the given accuracy level is specified in Table 4.

E. SPECIAL CASE DISTRIBUTIONS

The generalized nature of the distribution can derive many other fading models by setting the appropriate parameters as given in Table 5.

Thus, many other fading distributions can be approximated in terms of performance metrics. In the next section,

TABLE 5. Special cases.

Fading Model	η-μ Parameter
Rayleigh	$\eta = 1, \mu = 0.5$
Nakagami-m	$\eta \to 1, \mu = m/2; \eta \to 0, \mu = m$
Hoyt (Nakagami-q)	$\mu = 0.5$
One-sided Gaussian	$\eta \to 0, \mu = 0.5; \eta \to \infty, \mu = 0.5$

the results of validating and investigating the numerical behavior of the above derivation are presented.

V. RESULTS

To characterize the performance and behavior of the presented wireless communication system, the numerical results as PDF and CDF of the signal power are investigated. The proposed model performance is evaluated in three dimensions: 1-D for line topology, 2-D for circle topology, and 3-D for sphere topology. Each node transmits at unit power as discussed in the theoretical analysis. The results show a superior performance of the 1-D model compared to the 2-D and 3-D situations. The analysis of the OP and ABER metrics has been compared with the benchmark algorithms including, Nakagami-m, Nakagami-q (Hoyt), Rayleigh, and one-sided Gaussian distributions. Moreover, the fading characteristics of the received signal are analyzed in the NLOS using the η-μ fading model. Thus, the performance of the mobile network can be improved by analyzing the ABER and OP metrics for different fading models. Finally, to model the dynamic and mobile characteristics of wireless networks, the impact of noise-limited, interference-limited, and interference-plus-noise limited scenarios has been conducted.

In the numerical analysis, to analyze the fading characteristics of the wireless network, two strategies were considered while designing a link.

1) **Scenario 1:** In the first scenario, the value of the power at the transmitter is kept constant and the value of the SNR and fading vary over the distance D.
2) **Scenario 2:** The second scenario consists of a fixed average SNR at a finite distance D. The power is varied

$$P_{out}^{SINR} = \frac{2^{(1-2\mu_d)}}{h^{\mu_d}\Gamma(\mu_d)}\sqrt{\pi}\sum_{i=1}^{n}\frac{B_i}{(\beta_i+1)}\sum_{m=0}^{\infty}\frac{1}{m!\Gamma(\mu_d+m+\frac{1}{2})}\left(\frac{H}{2h}\right)^{2m}2\sqrt{\pi} \times\sum_{m=0}^{\infty}\frac{1}{m!\Gamma(\mu_c L+m+\frac{1}{2})}H^{2m}\sum_{j=0}^{2(\mu_d+m)}\binom{2\left(\mu_d+m\right)}{j} \times\frac{\Gamma\left(2\left(\mu_c L+m\right)+j\right)}{\Gamma\left(\mu_c L\right)}\left[\frac{2\mu_d h\theta}{\Omega_0}\right]^{2(\mu_d+m)}\left(\frac{\Omega_I}{2\mu_c}\right)^{j}\left(h^{-(\mu_c L+2m+j)}\right)2^{-2(\mu_c L+m)}\left\{\frac{1}{(2\mu_d+m)}\right. \times\Phi_1\left(2\left(\mu_d+m\right),2\left(\mu_c L+m\right)+j,2\left(\mu_d+m\right)+1,\left(\frac{-\mu_d\theta}{\mu_c\Lambda}\right),\frac{-2\mu_d h\theta}{\Omega_0}\right)-\frac{1}{\left(2\left(\mu_d+m\right)+\frac{\beta_i+1}{\varphi}\right)} \left.\times\Phi_1\left(2\left(\mu_d+m\right)\frac{\beta_i+1}{\varphi},2\left(\mu_c L+m\right)+j,2\left(\mu_d+m\right)+\frac{\beta_i+1}{\varphi}+1,\left(\frac{-\mu_d\theta y}{\mu_c\Lambda}\right),\frac{-2\mu_d h\theta}{\Omega_0}\right)\right\} \quad (45)$$

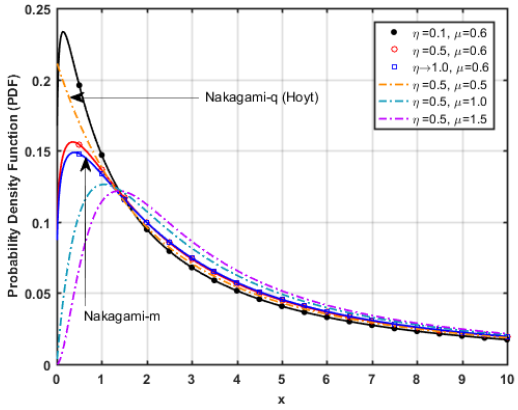

FIGURE 2. PDF of received power for a 1-D network with RWP mobility when $\eta = \{0.1, 0.5, 1.0\}$, $\mu = 0.6$, $\varphi = 3$ and $\mu = \{0.5, 1.0, 1.5\}$, $\eta = 0.5$, $\varphi = 3$. Solid line: η varying when μ is constant; dotted line: μ varying when η is constant.

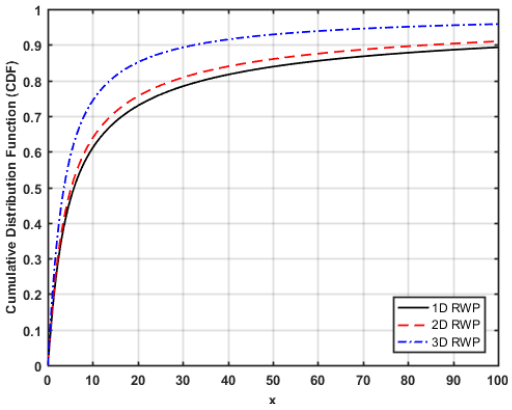

FIGURE 3. CDF of received power for different topologies of the RWP mobility model when $\eta = 0.5$, $\mu = 0.6$, $\varphi = 3$.

on the transmitter side to achieve a fixed value of average SNR at a distance D.

A. PDF AND CDF OF RECEIVED POWER

This section analyzes the PDF of the received power by varying the values of η-μ. The validity of the derived closed-loop expression is verified in Fig. 2 by comparing the theoretical PDF of the received power with the equations derived in equation (12) and in benchmark papers [41]. In both cases, the value of η is varied at a fixed value of μ, and varied μ at fixed η are plotted for the PDF. The values of the $\eta = \{0.1, 0.5, 1.0\}$ are varied at the constant value $\mu = 0.6$ to model the behavior of non-linearity in the environment, thereby keeping the number of multipath clusters constant. In the second case, the value of the $\mu = \{0.5, 1.0, 1.5\}$ is varied at a constant value of $\eta = 0.5$ to represent the behavior of many clusters with varied values. The value of the $\varphi = 3$ is kept constant at 3 in the numerical results.

Fig. 2 shows the validation and reveals that when the value of η is set at 1 and $\mu = \frac{m}{2}$, the PDF of received power shifts to a Nakagami-m model. Whereas, in case 2, for a value of $\mu = 0.5$, the Nakagami-q model characteristics are observed. Furthermore, with increasing value of the η, a right shift is observed in the graph showing a low probability of receiving power. The right shift trend in the graph can be observed with increasing value of the μ for a constant η environment. For case 2, a similar characteristic of right shift is observed with increasing the value of the μ for a constant η environment. It is observed in case 1 and 2 that when the value of the multipath cluster is kept constant with the increasing value of μ, an increase in the strength of received power is observed. Finally, it can be verified that the derived closed-loop expression has a more general form linked to other techniques as in [41] and can model the fading characteristic and dynamics of a next-generation network.

The next section analyzes the results obtained from the evaluation. The results are obtained using the 1-D topology. To examine the effect of different topologies, the CDF is plotted.

Fig. 3. shows the CDF characteristics of the received power as derived in equation (20) for different network topologies considering a random $\eta = 0.5, \mu = 0.6, \varphi = 3$ fading environment. The scenario with a unit transmit power is observed over a unit-normalized distance, $D = 1$. It can be depicted in Fig. 3 that the value of CDF of the 3-D distribution is higher than that of the 1-D and 2-D distributions. The right shift in the graph is observed while moving from the 3-D to 1-D distribution. The trend in the graph shows that a higher probability of received power is observed compared to 1-D and 2-D distributions. That is due to the modeling of the characteristics of expanded service areas in 3-D distribution. Yet, in [41], the modeling did not consider the effect of 3-D on the CDF. Our proposed distribution is more generalized and is not limited to Nakagami-m.

B. AVERAGE BIT ERROR RATE

The numerical analysis of the performance metrics is presented in this section. The analysis considered a mobile user moving in a maximum range of D = 100 m. For evaluation purposes, both of our link design scenarios are plotted in some cases, i.e., fixed average SNR and fixed transmit power at finite distance D. Moreover, in all cases, when the η and μ parameters are set, the behavior of many fading distributions, including Nakagami-m and Nakagami-q (Hoyt), can be analyzed as special cases. The evaluation parameters are as follows: $\eta = 0.5$, $\mu = 0.6$ when D = 100 m. A threshold ABER of 10^{-6} applies to further analysis.

This section shows the ABER with increasing transmit power. Path loss is an important parameter to model the effect of the ABER in a wireless system. Hence, to exhibit the dynamic characteristics of fading in the evaluation, in Fig. 4 the ABER as shown in equation (29) is depicted including the effect of the path loss exponent. The value of the path loss exponent $\varphi = \{2.0, 2.5, 3.0, 3.5\}$ is varied to evaluate the received signal behavior in different propagation environments.

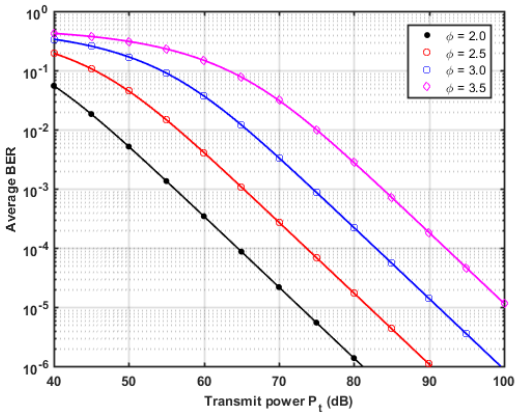

FIGURE 4. ABER of BPSK modulation for a 1-D network with RWP mobility when $\varphi = \{2.0, 2.5, 3.0, 3.5\}$, $\eta = 0.5$ and $\mu = 0.6$.

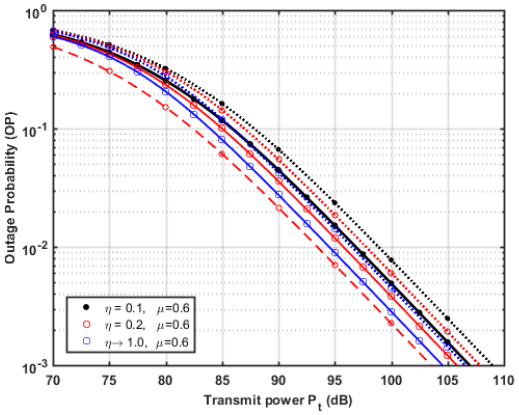

FIGURE 5. OP of received power when $\theta = 2$ for a 1-D network with RWP mobility while $\eta = \{0.1, 0.2, 1.0\}$, $\mu = 0.6$, and $\varphi = 4$. Solid line: Noise only; Dashed-dotted line: Interference only; Dotted line: Interference and noise.

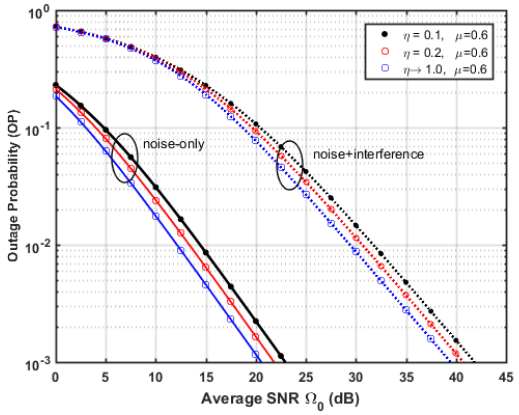

FIGURE 6. OP of received power when $\theta = 2$ for a 1-D network with RWP mobility when $\eta = \{0.1, 0.2, 1.0\}$, $\mu = 0.6$, $\varphi = 4$. Solid line: Noise only; Dotted line: Interference and noise.

The ABER value shows an increasing trend with rising path loss exponent values for a constant η and μ fading environment. The threshold value of ABER is noted to be 10^{-6} and is achieved at approximately 80 dBm when the value of $\varphi = 2.0$. This shows that with the increasing value of $\varphi = 2.0$, higher threshold values can be achieved according to the dynamic environmental conditions. A binary phase-shift keying (BPSK) modulation scheme is plotted against P_t analyzing the effect of bit error rate. Yet, the derived novel-form expression from the ABER in (29) is generic, so by varying the modulation parameters a and b, it is possible to get the desired ABER for various modulation schemes. The existing papers in [41] are not modeled in the dynamic environment in their derivation and thus cannot be used for analyzing the fading characteristics of wireless networks. The numerical results prove that the network designer can ease mobility and path loss on the ABER of a mobile user in an η-μ fading environment.

C. OUTAGE PROBABILITY

The OP of the received power is analyzed with transmit power P_t and Ω_0 for different heterogeneous environments having interferers and received signals.Moreover, the analysis uses an OP of 10^{-3} as reference for $\theta = 2$ which is the minimum threshold for power. The path loss exponent φ was kept constant at four while the fading parameters η and μ were varied for the analysis.

Figs. 5 and 6 illustrate the OP with the varying transmit power and average SNR, when the value of $\eta = \{0.1, 0.2, 1.0\}$ and value of constant multipath cluster is $\mu = 0.6$ for $\varphi = 4$. The analysis of the OP is done for the noise-limited, interference-limited, and interference+ noise systems cases to analyze their behaviors.

Fig. 5 shows the effect of different parameters on the OP performance. The OP value is high when the effect of noise and interference is modeled in the results as shown.

It depicts that, for all environments, the system performance increases by increasing the value of η for wireless systems. For all the combinations of η and μ, the performance of an interference-limited system is the best even though the environment with noise performs well compared to the one that has noise-with-interference systems. Thus, the proposed derivations show a clear relationship of varying the η and μ values on the OP, and network designers can model the effect of interference and noise by changing the values of η and μ to improve the performance of the wireless system.

In Fig. 6 analysis is done for designing the link keeping a fixed average SNR at a distance D. Here, the transmitted power is varied to maintain a fixed SNR in different fading environments. On OP, a similar trend is observed as in the case of Fig. 5. For these plots, interferers with identical interference-to-noise ratio of $\Omega_I = P_I d_I^{-\varphi} = 10$ dBm are applied. When the fading parameter η is characterized, the performance increases with rising η. To achieve an OP of 10^{-3} when $\varphi = 4$, $\eta = \{0.1, 0.2, 1\}$ the fading environments need average SNR values of approximately 20, 22, and 23 dBm, in the presence of noise only. When noise and interference are counted, the same system needs average SNR values of 39, 40, and 42 dBm. Moreover, transmit powers needed to achieve this value of average SNR at distance D

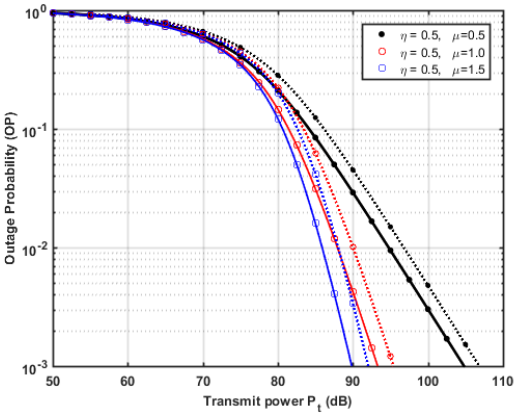

FIGURE 7. OP of received power versus transmit power when $\theta = 2$ for a 1-D network when $\varphi = 4$, $\mu = \{0.5, 1.0, 1.5\}$, $\eta = 0.5$. Solid line: Noise only; Dotted line: Interference and noise.

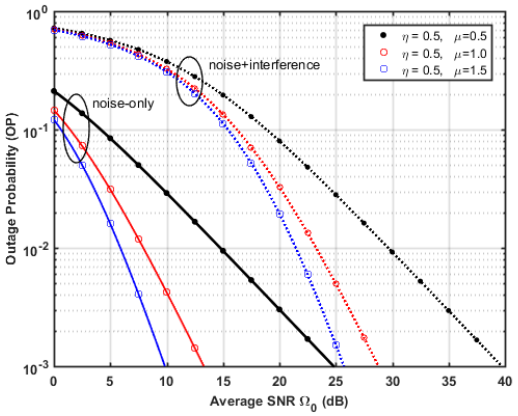

FIGURE 8. OP of received power versus average SNR when $\theta = 2$ for a 1-D network when $\varphi = 4$, $\mu = \{0.5, 1.0, 1.5\}$, $\eta = 0.5$. Solid line: Noise only; Dotted line: Interference and noise.

can be calculated using $\Omega_0 = P_t D^{-\varphi}$ and the relationship $\Lambda = \frac{P_t}{P_l}$. Thus, the closed-loop expression shows that by varying η and μ parameters in different environments, such as extreme wireless networks, the performance can be improved on designing the wireless networks. Thus, the benchmark papers [41] cannot model the mobility and dynamic nature of the wireless networks.

To model a real-scenario for a dynamic wireless network, we evaluate with a mobile node in an $\eta = 0.2$, $\mu = 0.6$, $\varphi = 4$ environment with a maximum range of $D = 100\ m$ when transmit power is 100 dBm. The system is seen to have an OP of about 4×10^{-3} when the system is modeled with noise, while it is about 2×10^{-3} for an interference-limited system. When the transmission occurs in the presence of both noise and interference, an OP of about 6×10^{-3} is observed under similar conditions. Thus, the derived closed-loop expression can show that the fading phenomenon has diverse characteristics in wireless networks and can be taken into consideration while designing a network.

D. VARYING MULTIPATH CLUSTERS

This section analyzes the OP behavior for varying multipath clusters keeping the value of the non-linearity constant η fixed. Fig. 7 plots the OP for a fixed power link design in a constant $\eta = 0.5$ fading environment. Fig. 7 illustrates that with an increase in the value of μ, the performance of the system increases. The performance of the OP decreases when the system is modeled with interference and noise. As a result, a clear relationship between noise and interference is modeled in the derivation. The OP of varying multipath clusters μ in fixed η environments is illustrated for the second scenario in Fig. 8 whose behavior is similar to Fig. 6 so that with an increasing value of μ, the value of the OP increases. Similarly, when interference and noise are added to the system, the system performance decreases due to different fading and mobility characteristics of the wireless network.

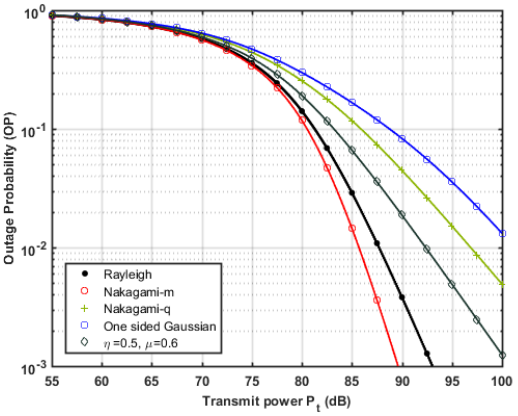

FIGURE 9. OP of received power when $\theta = 2$ in a 1-D network model at $\varphi = 4$ for a noise-limited system.

E. SPECIAL CASE PROOF

In Fig. 9. the graph of OP is depicted, which incorporates the RWP mobility model for characterizing dynamic fading distributions as modeled in the generalized η-μ distribution. All special cases are obtained using format 1 of the distribution. However, by substituting suitable parameters, format 2 can also be used for such special case approximations. Nakagami-m distribution is obtained by setting $\eta = 1$, $\mu = \frac{m}{2}$ where m is 1.5 in this case, and Nakagami-q (Hoyt) is obtained with $\eta = q$, $\mu = 0.5$. In this depiction, q is taken to be 0.1. One-sided Rayleigh and Gaussian distribution can be derived from the Nakagami-m model by incorporating the value of $m = 0.5$ and $m = 1$, respectively [44]. The performance analysis of the mobility incorporating the different distributions can be considered a special case. The proposed model is also presented as flexible and adaptive with the mobility behavior of various dynamic wireless fading environments by varying the values of η and μ parameters, whereas the fading characteristics in [41] have not included the mobility characteristics of wireless networks. The paper [41] may have considered similar characteristics

with the value of $\mu = 0.5$ in the Nakagami-m model. However, in our proposed scenario, the novel-form expressions for the received power of the wireless environment by incorporating the mobility characteristics are not limited to the Nakagami-m distribution.

VI. CONCLUSION

Generalized novel-form expressions for the PDF and CDF of the received power is proposed including the ABER and OP metrics in a dynamic wireless network following the RWP mobility design in an η-μ fading distribution. Performance of the proposed fading model was analyzed in PDF and CDF for 1-D, 2-D, and 3-D network deployment structures. An ABER evaluation for generic modulations was provided. The validation results of the analytical expressions show that the proposed novel-form expression can be used for investigating the effect of fading for different dynamic environments.

APPENDIX A
TWO $\eta - \mu$ DISTRIBUTION FORMATS

Here are the two different formats of the η-μ fading channel as described in [50], [51].

Format 1: The fading signals are independent within each cluster and have different values of power,

$$H = \frac{\eta^{-1} - \eta}{4}; \quad h = \frac{2 + \eta^{-1} + \eta}{4}; \ \eta > 0 \tag{46}$$

where $0 < \eta < \infty$ represents the wave power ratio.

Format 2: Received power of the fading signal is correlated and identical within each cluster represented by,

$$H = \frac{\eta}{1 - \eta^2}; \quad h = \frac{1}{1 - \eta^2}; \ -1 \le \eta \le 1 \tag{47}$$

where $-1 < \eta < 1$, is representing correlation coefficient between the quadrature components and each multipath cluster.

APPENDIX B
DERIVATION OF (35)

The relationship in [45] equation (6.455.2) can be seen in equation (25).

The expression in (34) can be simplified and arranged into

$$\begin{aligned} C_1 = {} & \frac{2\sqrt{\pi}}{\Gamma(\mu_c L)} \left(\frac{\mu_c}{\Omega_I}\right)^{2\mu_c L} h^{\mu_c L} \\ & \times \sum_{m=0}^{\infty} \frac{1}{m!\Gamma(\mu_c L + m + \frac{1}{2})} \left(\frac{\mu_c H}{\Omega_I}\right)^{2m} \\ & \times \frac{\left(\frac{2\mu_d h\theta}{\Omega_0}\right)^{2(\mu_d+m)} \Gamma\left(2\mu_c L + 2m + 2\mu_d + 2m\right)}{2\left(\mu_d + m\right)\left(\frac{2\mu_d h\theta}{\Omega_0} + \frac{2\mu_c h}{\Omega_I}\right)^{2(\mu_c L + \mu_d + 2m)}} \\ & \times {}_2F_1\left(1, 2\left(\mu_c L + \mu_d + 2m\right); 2\left(\mu_d + m\right) + 1; \right. \\ & \left. \left(\frac{\frac{2\mu_d h\theta}{\Omega_0}}{\frac{2\mu_d h\theta}{\Omega_0} + \frac{2\mu_c h}{\Omega_I}}\right)\right). \end{aligned} \tag{48}$$

APPENDIX C
DERIVATION OF (41)

The expression in (40) can be expanded using the incomplete gamma function relationship below

$$\gamma\left(v, x\right) = x^v \int_0^1 y^{(v-1)} e^{-xy} dy. \tag{49}$$

Considering [47], the expression in [40], can then be expressed as follows considering the binomial expansion given in [52]

$$(1 + x)^n = \sum_{k=0}^{n} {}_nC_k x^k = \sum_{k=0}^{n} \binom{n}{k} x^k. \tag{50}$$

Then, using (50), the expression in [40] can be expressed as

$$\begin{aligned} K_1 = {} & \frac{2\sqrt{\pi}}{\Gamma(\mu_c L)} h^{\mu_c L} \sum_{m=0}^{\infty} \frac{H^{(2m)}}{m!\Gamma(\mu_c L + m + \frac{1}{2})} \\ & \times \left[\frac{\mu_c}{\Omega_I}\right]^{2(\mu_c L + m)} H^{2m} \left[\frac{2\mu_d h\theta}{\Omega_0}\right]^{2(\mu_d + m)} \\ & \times \int_0^1 y^{(2(\mu_d+m)-1)} exp\left[-\left(\frac{2\mu_d h\theta}{\Omega_0} y\right)\right] \\ & \times \sum_{j=0}^{2(\mu_d+m)} \binom{2\left(\mu_d + m\right)}{j} \\ & \times \int_0^{\infty} x^{(2\mu_c L + 2m + j - 1)} \\ & \times exp\left(-x\left(\frac{2\mu_c h}{\Omega_I} + \frac{2\mu_c h\theta y}{\Omega_0}\right)\right) dxdy. \end{aligned} \tag{51}$$

The solution for the integral of the following form can be expressed using [45] equation (3.326.2)

$$\int_0^{\infty} x^m exp\left(-\beta x^n\right) dx = \frac{\Gamma\left(\gamma\right)}{n\beta^{\gamma}} \tag{52}$$

where $\gamma = \left(\frac{m+1}{n}\right)$.

Solving the integral in (51) using the results of (52) are

$$\begin{aligned} K_1 = {} & \frac{2\sqrt{\pi}}{\Gamma(\mu_c L)} h^{\mu_c L} \sum_{m=0}^{\infty} \frac{1}{m!\Gamma(\mu_c L + m + \frac{1}{2})} \\ & \times H^{2m} \sum_{j=0}^{2(\mu_d+m)} \binom{2\left(\mu_d + m\right)}{j} \\ & \times \left[\frac{2\mu_d h\theta}{\Omega_0}\right]^{2(\mu_d+m)} \Gamma\left(2\mu_c L + 2m + j\right) \\ & \times \left(2h + \frac{2\mu_d h\theta}{\mu_c \Lambda} y\right)^{-2(\mu_c L + m)} \\ & \times \frac{\left(\frac{\Omega_I}{\mu_c}\right)^j}{\left(2h + \frac{2\mu_d h\theta y}{\mu_c \Lambda}\right)^j} \int_0^1 y^{2(\mu_d+m)-1} \\ & \times exp\left[-\left(\frac{2\mu_d h\theta}{\Omega_0} y\right)\right] dy \end{aligned} \tag{53}$$

where $\Lambda = \left(\frac{\Omega_0}{\Omega_I}\right)$.

By factorizing and rearranging, the expression in (53) in the form of (41) is obtained.

REFERENCES

[1] I. F. Akyildiz, A. Kak, and S. Nie, "6G and beyond: The future of wireless communications systems," *IEEE Access*, vol. 8, pp. 133995–134030, 2020.

[2] L. U. Khan, I. Yaqoob, M. Imran, Z. Han, and C. S. Hong, "6G wireless systems: A vision, architectural elements, and future directions," *IEEE Access*, vol. 8, pp. 147029–147044, 2020.

[3] Y. Ogawa, M. Umehira, and X. Wang, "Kriging-based RSSI prediction for cell coverage discovery using spectrum database in 5G multi-band cellular networks," in *Proc. 23rd Asia–Pacific Conf. Commun. (APCC)*, Dec. 2017, pp. 1–5.

[4] A. M. Pessoa, I. M. Guerreiro, C. F. M. E. Silva, T. F. Maciel, D. A. Sousa, D. C. Moreira, and F. R. P. Cavalcanti, "A stochastic channel model with dual mobility for 5G massive networks," *IEEE Access*, vol. 7, pp. 149971–149987, 2019.

[5] C. Sergiou, M. Lestas, P. Antoniou, C. Liaskos, and A. Pitsillides, "Complex systems: A communication networks perspective towards 6G," *IEEE Access*, vol. 8, pp. 89007–89030, 2020.

[6] T. Huang, W. Yang, J. Wu, J. Ma, X. Zhang, and D. Zhang, "A survey on green 6G network: Architecture and technologies," *IEEE Access*, vol. 7, pp. 175758–175768, 2019.

[7] L. Chettri and R. Bera, "A comprehensive survey on Internet of Things (IoT) toward 5G wireless systems," *IEEE Internet Things J.*, vol. 7, no. 1, pp. 16–32, Jan. 2020.

[8] I. Vilà, J. Pérez-Romero, O. Sallent, and A. Umbert, "Characterization of radio access network slicing scenarios with 5G QoS provisioning," *IEEE Access*, vol. 8, pp. 51414–51430, 2020.

[9] Q. Zhang, H. H. Yang, T. Q. Quek, and J. Lee, "Heterogeneous cellular networks with LoS and NLoS transmissions—The role of massive MIMO and small cells," *IEEE Trans. Wireless Commun.*, vol. 16, no. 12, pp. 7996–8010, Sep. 2017.

[10] T. H. Nguyen, W.-S. Jung, L. T. Tu, T. V. Chien, D. Yoo, and S. Ro, "Performance analysis and optimization of the coverage probability in dual hop LoRa networks with different fading channels," *IEEE Access*, vol. 8, pp. 107087–107102, 2020.

[11] O. Ozdogan, E. Björnson, and E. G. Larsson, "Massive MIMO with spatially correlated Rician fading channels," *IEEE Trans. Commun.*, vol. 67, no. 5, pp. 3234–3250, May 2019.

[12] C. A. Gutiérrez, J. T. Gutiérrez-Mena, J. M. Luna-Rivera, D. U. Campos-Delgado, R. Velazquez, and M. Patzold, "Geometry-based statistical modeling of non-WSSUS mobile-to-mobile Rayleigh fading channels," *IEEE Trans. Veh. Technol.*, vol. 67, no. 1, pp. 362–377, Jan. 2018.

[13] A. A. Dos Anjos, T. R. R. Marins, C. R. Nogueira Da Silva, V. M. R. Peñarrocha, L. Rubio, J. Reig, R. A. A. De Souza, and M. D. Yacoub, "Higher order statistics in a mmWave propagation environment," *IEEE Access*, vol. 7, pp. 103876–103892, 2019.

[14] H. H. Yang, A. Arafa, T. Q. S. Quek, and V. Poor, "Optimizing information freshness in wireless networks: A stochastic geometry approach," *IEEE Trans. Mobile Comput.*, early access, Feb. 28, 2020, doi: 10.1109/TMC.2020.2977010.

[15] M. G. Kibria, K. Nguyen, G. P. Villardi, W.-S. Liao, K. Ishizu, and F. Kojima, "A stochastic geometry analysis of multiconnectivity in heterogeneous wireless networks," *IEEE Trans. Veh. Technol.*, vol. 67, no. 10, pp. 9734–9746, Oct. 2018.

[16] H. Al-Hmood and H. S. Al-Raweshidy, "Unified modeling of composite κ-μ/gamma, $\eta - \mu$/gamma, and $\alpha - \mu$/gamma fading channels using a mixture gamma distribution with applications to energy detection," *IEEE Antennas Wireless Propag. Lett.*, vol. 16, pp. 104–108, 2017.

[17] C. B. Issaid, M.-S. Alouini, and R. Tempone, "On the fast and precise evaluation of the outage probability of diversity receivers over $\alpha-\mu$, $\kappa-\mu$, and $\eta-\mu$ fading channels," *IEEE Trans. Wireless Commun.*, vol. 17, no. 2, pp. 1255–1268, Dec. 2017.

[18] N. Sharma, A. Bansal, and P. Garg, "Decode-and-forward relaying in mixed $\eta - \mu$ and gamma–gamma dual hop transmission system," *IET Commun.*, vol. 10, no. 14, pp. 1769–1776, Sep. 2016.

[19] S. Nallagonda, G. K. Kumar, and A. K. Nallagonda, "Comprehensive performance analysis of data-fusion aided cooperative cognitive radio network over $\eta-\mu$ fading channel," *IET Commun.*, vol. 13, no. 16, pp. 2558–2566, Oct. 2019.

[20] M. K. Kundu, A. S. Sumona, A. S. M. Badrudduza, and S. Shabab, "Analysis of secrecy performance over correlated $\eta - \mu$ fading channels," in *Proc. IEEE Int. Conf. Signal Process., Inf., Commun. Syst. (SPICSCON)*, Nov. 2019, pp. 100–103.

[21] D. Dixit and P. R. Sahu, "Performance of dual-hop DF relaying systems with QAM schemes over mixed $\eta - \mu$ and $\kappa - \mu$ fading channels," *Trans. Emerg. Telecommun. Technol.*, vol. 28, no. 11, p. e3179, Nov. 2017.

[22] O. S. Badarneh, F. S. Almehmadi, I. S. Ansari, and X. Yang, "Wireless energy harvesting in cooperative decode-and-forward relaying networks over mixed generalized $\eta - \mu$ and $\kappa - \mu$ fading channels," *Trans. Emerg. Telecommun. Technol.*, vol. 29, no. 2, p. e3262, Feb. 2018.

[23] J. Y. L. Chen and X. Lei, "Dual-hop cognitive amplify-and-forward relaying networks over $\eta - \mu$ fading channels," *IEEE Trans. Veh. Technol*, vol. 65, pp. 6290–6300, 2016.

[24] O. S. Badarneh and R. Mesleh, "Cooperative dual-hop wireless communication systems with beamforming over $\eta - \mu$ fading channels," *IEEE Trans. Veh. Technol.*, vol. 65, no. 1, pp. 37–46, Jan. 2016.

[25] M. Surendar, S. S. Rajput, and P. Muthuchidambaranathan, "Symbol error rate of QO-STBC based decode-and-forward cooperative communication system over generalised $\eta - \mu$ and $\kappa - \mu$ fading channels," *IET Commun.*, vol. 11, no. 9, pp. 1379–1386, Jun. 2017.

[26] Y. J. Chun, S. L. Cotton, H. S. Dhillon, A. Ghrayeb, and M. O. Hasna, "A stochastic geometric analysis of device-to-device communications operating over generalized fading channels," *IEEE Trans. Wireless Commun.*, vol. 16, no. 7, pp. 4151–4165, Jul. 2017.

[27] M. Srinivasan and S. Kalyani, "Analysis of MRC with $\eta - \mu$ co-channel interference," *IEEE Trans. Veh. Technol.*, vol. 69, no. 1, pp. 738–745, Nov. 2020.

[28] L. Yang, M. O. Hasna, and I. S. Ansari, "Physical layer security for TAS/MRC systems with and without co-channel interference over $\eta - \mu$ fading channels," *IEEE Trans. Veh. Technol.*, vol. 67, no. 12, pp. 12421–12426, Oct. 2018.

[29] N. Y. Ermolova and O. Tirkkonen, "Outage probability analysis in generalized fading channels with co-channel interference and background noise: $\eta - \mu/\eta - \mu$, $\eta - \mu/\kappa - \mu$, and $\kappa - \mu/\eta - \mu$ scenarios," *IEEE Trans. Wireless Commun.*, vol. 13, no. 1, pp. 291–297, Jan. 2014.

[30] S. Kumar and S. Kalyani, "Coverage probability and rate for $\eta - \mu$ fading channels in interference-limited scenarios," *IEEE Trans. Wireless Commun*, vol. 14, pp. 6082–6096, 2015.

[31] H. Tabassum, M. Salehi, and E. Hossain, "Mobility-aware analysis of 5G and B5G cellular networks: A tutorial," 2018, *arXiv:1805.02719*. [Online]. Available: http://arxiv.org/abs/1805.02719

[32] M. Banagar and H. S. Dhillon, "Performance characterization of canonical mobility models in drone cellular networks," *IEEE Trans. Wireless Commun.*, vol. 19, no. 7, pp. 4994–5009, Jul. 2020.

[33] R. Amer, W. Saad, and N. Marchetti, "Mobility in the sky: Performance and mobility analysis for cellular-connected UAVs," *IEEE Trans. Commun.*, vol. 68, no. 5, pp. 3229–3246, May 2020.

[34] C. Bettstetter, G. Resta, and P. Santi, "The node distribution of the random waypoint mobility model for wireless ad hoc networks," *IEEE Trans. Mobile Comput.*, vol. 2, no. 3, pp. 257–269, Jul. 2003.

[35] S. Althunibat, O. S. Badarneh, and R. Mesleh, "Random waypoint mobility model in space modulation systems," *IEEE Commun. Lett.*, vol. 23, no. 5, pp. 884–887, May 2019.

[36] O. S. Younes and U. A. Albalawi, "Analysis of route stability in mobile multihop networks under random waypoint mobility," *IEEE Access*, vol. 8, pp. 168121–168136, 2020.

[37] A. A. Khuwaja, Y. Chen, and G. Zheng, "Effect of user mobility and channel fading on the outage performance of UAV communications," *IEEE Wireless Commun. Lett.*, vol. 9, no. 3, pp. 367–370, Mar. 2020.

[38] S. Bandyopadhyay, E. J. Coyle, and T. Falck, "Stochastic properties of mobility models in mobile ad hoc networks," *IEEE Trans. Mobile Comput.*, vol. 6, no. 11, pp. 1218–1229, Nov. 2007.

[39] M. Comisso and F. Babich, "Coverage analysis for 2D/3D millimeter wave peer-to-peer networks," *IEEE Trans. Wireless Commun.*, vol. 18, no. 7, pp. 3613–3627, Jul. 2019.

[40] K. Govindan, K. Zeng, and P. Mohapatra, "Probability density of the received power in mobile networks," *IEEE Trans. Wireless Commun.*, vol. 10, no. 11, pp. 3613–3619, Nov. 2011.

[41] V. A. Aalo, C. Mukasa, and G. P. Efthymoglou, "Effect of mobility on the outage and BER performances of digital transmissions over Nakagami-*m* fading channels," *IEEE Trans. Veh. Technol.*, vol. 65, no. 4, pp. 2715–2721, Apr. 2016.

[42] C. Mukasa, V. A. Aalo, and G. Efthymoglou, "Performance analysis of a mobile receiver in a field of Poisson interferers," in *Proc. IEEE 38th Sarnoff Symp.*, Sep. 2017, pp. 1–6.
[43] C. Li, J. Yao, H. Wang, U. Ahmed, and S. Du, "Effect of mobile wireless on outage and BER performances over Rician fading channel," *IEEE Access*, vol. 8, pp. 91799–91806, 2020.
[44] S. Panic, M. Stefanovic, J. Anastasov, and P. Spalevic, *Fading and Interference Mitigation in Wireless Communications*. Boca Raton, FL, USA: CRC Press, 2017. [Online]. Available: https://doi.org/10.1201/b16275
[45] I.Gradshteyn and I. M. Ryzhik, *Tables of Integrals, Series, and Products*, 6th ed. New York, NY, USA: Academic, 2000.
[46] F. S. Almehmadi and O. S. Badarneh, "Performance analysis of outage probability and error rate of square M-QAM in mobile wireless communication systems over generalized $\alpha - \mu$ fading channels with non-Gaussian noise," *China Commun.*, vol. 15, no. 1, pp. 62–71, Jan. 2018.
[47] C. Mukasa, V. A. Aalo, and G. Efthymoglou, "On the performance of a dual-hop network with a mobile relay in a nakagami fading environment," in *Proc. IEEE 21st Int. Workshop Comput. Aided Modeling Design Commun. Links Netw. (CAMAD)*, Oct. 2016, pp. 43–47.
[48] A. Goldsmith, *Wireless Communications*. Stanford, CA, USA: Stanford Univ., 2004.
[49] M. D. Yacoub, G. Fraidenraich, H. B. Tercius, and F. C. Martins, "The symmetrical $\eta - \kappa$ distribution: A general fading distribution," *IEEE Trans. Broadcast.*, vol. 51, no. 4, pp. 504–511, Nov. 2005.
[50] D. B. da Costa and M. D. Yacoub, "The $\eta - \mu$ joint phase-envelope distribution," in *Proc. IEEE Wireless Commun. Netw. Conf.*, Mar. 2007, pp. 1906–1908.
[51] C. Priyanka and V. Nithya, "Physical scenario perusal of $\eta-\mu$ fading channels," in *Proc. Int. Conf. Commun. Signal Process. (ICCSP)*, Apr. 2015, pp. 0708–0712.
[52] E. Michael, "Module 6 the binomial theorem," in *Algebra and Coordinate. Geometry*. Melbourne, VIC, Australia: Education Services Australia, 2013.

EKKAPHOT MEESA-ARD received the M.Eng. degree in electrical and information engineering from the King Mongkut's University of Technology Thonburi, Bangkok, Thailand, in 2012, where he is currently pursuing the Ph.D. degree in electrical and information engineering. He is interested in the performance analysis of wireless communication systems. His current research interests include mobile communications, fading channels, interference mitigation of device-to-device communications, evaluating the impact of mobility on 5G networks, and the modeling of smart Internet of Things.

SUWAT PATTARAMALAI was born in Bangkok, Thailand, in 1969. He received the B.E.E. degree in electrical engineering from Chulalongkorn University, Bangkok, in 1991, and the M.Eng. and Ph.D. degrees in electrical engineering from Florida Atlantic University, Boca Raton, in 1996 and 2007, respectively. Since 1993, he has been with the Department of Electronic and Telecommunication Engineering, Faculty of Engineering, King Mongkut's University of Technology Thonburi, Bangkok. His research interests include digital communications, fading channels, performance analysis of wireless networks, and modeling of cellular systems.